25·29 August 2024
inter.noise
NANTES FRANCE

Acoustic characterization of porous windscreens

Ashwin Sadanand Nayak [1], Andrés Prieto[2],
Universidade da Coruña
Campus de Elviña, 15008 A Coruña.

Daniel Fernández-Comesaña[3],
Microflown Technologies,
Tivolilaan, 6824BV Arnhem, The Netherlands.

ABSTRACT

Acoustic measurements of ground vehicles, wind turbines or aircrafts are often performed outdoors in presence of wind. Air movement around an acoustic sensor can significantly impact measurements due to flow-induced vibrations and turbulence. This is specially relevant for pressure-gradient and particle-velocity based acoustic transducers which are more sensitive to these perturbations. To attenuate this effect and improve measurement quality, the sensors are typically covered with windscreens made of porous materials. However, designing an appropriate windscreen poses a challenging task, demanding a deep understanding of sound transmission characteristics. This study works towards quantifying acoustic properties of rigid-frame porous materials through in-situ measurements and fitting a parametric fluid-equivalent model to find optimal model parameters. The parameters are subsequently investigated by comparing windscreen insertion loss through finite-element numerical simulations and measurements on a sound intensity PU probe.

1. INTRODUCTION

Practical applications in measuring acoustic signals often involve unexpected difficulties. Sound sources can be physically inhibiting or in motion, preventing measurements in its proximity. Noise measurements related to ground vehicles, wind turbines and aircrafts are necessarily performed in outdoor environments, in presence of natural elements like wind or rain. These situations often require testing procedures adapted to each specific case. Specifically, additional sensor shielding is necessary for outdoor measurements in presence of wind. Air flow may induce noise in the sensor due to turbulence and can also pose problems in quantifying the acoustic field [1, 2]. The susceptibility of an acoustic sensor to wind noise is dependent on its mechanical design and transduction principle. Pressure-gradient and particle-velocity based acoustic transducers exhibit more flow-induced noise than pressure-based transducers [2–4]. To attenuate this noise and improve measurement quality, the sensors are covered in windscreens. An effective design requires a thorough understanding of sound transmission through windscreens to ensure accurate measurements.

[1]ashwinsnayak@gmail.com

[2]andres.prieto@udc.es

[3]fernandez@microflown.com

The earliest microphone windscreen designs were silk-wrapped cages patented by Thorne [5] and Spotts [6]. These were inspired by theoretical studies of Phelps [7] who utilized Bernoulli's principle for air pressure around a spherical microphone assembly. The windscreens had a spherical form factor attributed to direction-neutrality towards wind noise attenuation. Hosier and Donavan [8] investigated performance of ten different microphone windscreens in their report, highlighting key descriptors for windscreen design: *wind-induced noise*, referring to the noise produced by air flow around the structure and *acoustic insertion loss*, indicating the difference in sound pressure levels that were induced by their presence on the sensor. Additional studies [9] indicated foam materials perform better in attenuating noise and subsequent windscreen designs have preferred porous foam materials for their structural characteristics and better signal-to-noise ratio (SNR). Recent literature in windscreen designs have been specific to their target applications introducing with them particular design challenges. Consider for example, noise measurements in a wind farm where large wind-turbines produce higher acoustic emission levels in presence of wind. These measurements can only be performed outdoors, away from the source and with significant air flow around the sensor. Choosing the right porous material and windscreen geometry is imperative in such conditions. Studies have indicated improved effectiveness with hollowed secondary windscreens over the primary windscreens enclosing a layer of air to reduce air flow [10]. Hansen et al. [11] compared the effectiveness of three radically different secondary windscreen designs- hemispherical, spherical and box buried into the earth. While the different designs showed varied degree of sound attenuation, measuring their insertion losses were instrumental in choosing them. Novak et al. [12] demonstrated the benefits of secondary windscreens over using just the primary, and compared the performance of commercially available secondary windscreen designs for wind-turbine measurements. The study cited lack of data with regard to the insertion loss of the secondary windscreens to remark on the varied behavior of noise attenuation. More recently, similar studies were also performed in Germany by Kirsch [13] and Martens et al. [14] towards the development of a secondary windscreens as a remedy to improve SNR ratio in wind turbine measurements. While the investigations emphasize on certain constructions of windscreen for particular measurement scenarios, the choice of windscreen material and geometry has largely followed an empirical design approach. Therefore, there exists a significant interest, particularly in sensor applications, for an in-depth study of the acoustical behavior of the windscreens.

The standard methodologies, the acoustical performance of porous materials are measured using surface absorption and impedance measurements of the sample conducted either in a Kundt's tube (ISO 10534 and ASTM E1050) or a reverberant room (ISO 354 and ASTM C423) under laboratory conditions. On the other hand, there are recent studies in a more non-destructive in-situ methodologies, such as the P-U "in-situ" method, which have demonstrated to yield similar results [15]. Many applications warrant ad-hoc measurements that quantify acoustic properties especially in room acoustics [16, 17]. Since the control parameters of interest are geometry and material properties of windscreen, the objective is to develop a high-fidelity simulation tool to prototype windscreen design.

This article focuses on developing a workflow that first retreives the insertion loss behavior of windscreen geometry by characterizing the acoustical properties of the material, and then applies finite element simulations. The insertion loss for windscreens made of different materials are measured by insitu measurements using an intensity probe. The behavior is sought to be recreated *in-silico* by finite element models. The parameters used in the simulation are obtained by inverse characterization of the surface impedance of the porous material. The acoustic parameters of the material are quantified by data-fitting to a parametric model for surface impedance.

2. MEASURING WINDSCREEN INSERTION LOSS

Two different windscreens made of foam were fabricated and a simple experimental setup was used to quantify their insertion loss. The porous foam windscreens are cylindrical in shape and made of two different materials, namely the EKI Melamine and EKI Filter Foam 90 PPI (see Figure 1a). The outer radius of the cylinder was 20mm and the height was 70mm and was designed to encapsulate the sensor in between without any noticeable air gap. The sensor used is the 0.5-inch cylindrical Microflown PU intensity probe mounted vertically. Measurements were performed within the inhouse anechoic chamber at Microflown Technologies which included absorbers on the surrounding walls to prevent any external influences and also prevent any reflections. A sound source was placed perpendicular to the direction of the probe pillars where the probe is most sensitive (see Figure 1b and 1c). The usual mount to afix the probe on the speaker housing was deemed short (due to plane-wave approximations) and hence, the probe was placed at an approximate distance of 1.5m from the speaker. Broadband white noise was used as the sound signal for an interval of 30 seconds and the associated pressure and particle velocity spectra were obtained. Subsequently, foam windscreens were introduced over the probe and the experiments were repeated. Multiple trials were conducted to ensure the consistency of measurements and minimize the re-positioning bias.

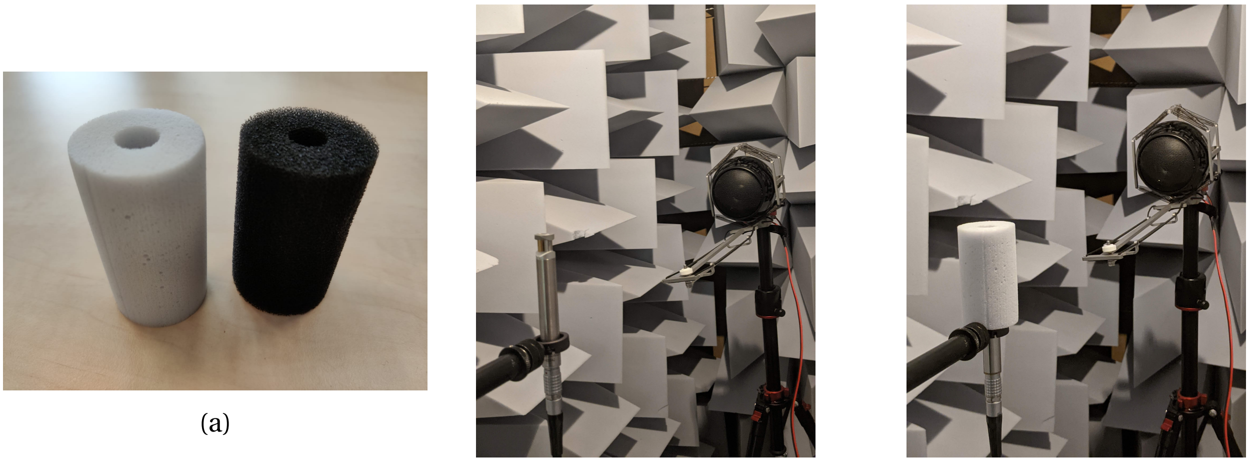

(a) (b) (c)

Figure 1: Cylindrical windscreen made of EKI Melamine (light blue) and EKI Filter Foam (black) were used to measure insertion loss (a). Measurement setup of probe and speaker with (b) and without (c) the porous windscreen in an anechoic chamber.

The pressure and particle velocity fields with and without windscreens are presented in Figure 2. The windscreens show significant differences primarily at high frequencies (>5 kHz) with both pressure and particle velocity fields having different losses. However, it is noted that at lower frequencies up to 1000 Hz, the pressure sensor does not display any variations but particle velocity fields clearly display varied losses between the two materials. Frequencies below 100 Hz were omitted due to the limitations of the testing environment (cut-off frequency of 100 Hz). A high repeatability is observed between different trials shown by the standard-deviation bars around the mean measurement. From these results, it is inferred that the selection of windscreen materials has a significant impact on the sensor performance, especially in particle velocity transducers, and the right choice of windscreen material and geometry is more critical.

3. PREDICTING WINDSCREEN INSERTION LOSS

This section aims to recreate the insertion loss behavior through parametric characterization of the acoustic behavior of windscreens. A wide range of porous material models provide the material response along a range of frequencies. The popular parametric models in literature

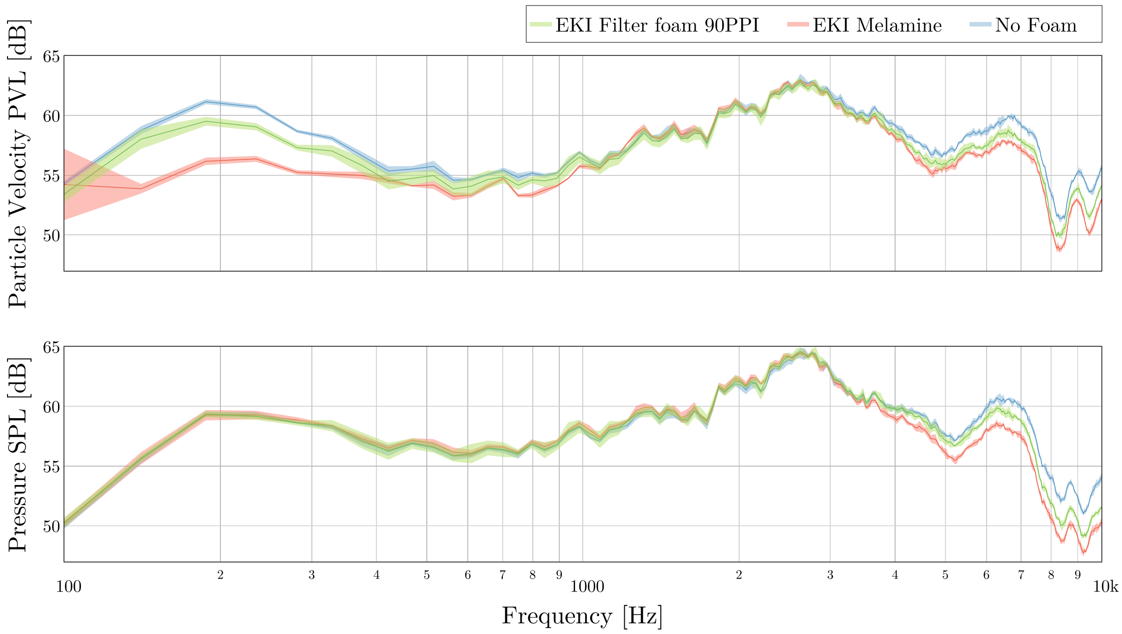

Figure 2: Experimental measurement of particle velocity and pressure with and without porous layer.

are Zwikker-Kosten model [18], Delany-Bazley model [19] and Delany-Bazley-Miki model [20] based on one parameter, Darcy's-like model [21, 22] based on two parameters, general Miki model [20] and Attenborough model [23] and Wilson model [24] based on four parameters, Johnson-Champoux-Allard model [25, 26] based on five parameters, Johnson-Champoux-Allard-Lafarge [25–27] model based on six parameters, and Johnson-Champoux-Allard-Pride-Lafarge [25–28] model based on eight parameters.

While any parametric model be used in a similar manner, the fairly detailed six-parameter Johnson-Champoux-Allard-Lafarge (JCAL) model is chosen in the current study. The model is reliable for porous materials with rigid frames and arbitrarily shaped pores and provides nonlinear expressions to compute the frequency-dependent dynamic porous mass density and bulk modulus, given as,

$$\rho_{\mathrm{P}}(\omega;\boldsymbol{\theta}) = \frac{\rho_{\mathrm{F}}}{\phi}\alpha_\infty\left(1-\mathrm{i}\frac{\sigma\phi}{\omega\rho_{\mathrm{F}}\alpha_\infty}\sqrt{1+\mathrm{i}\frac{4\alpha_\infty^2\eta\rho_{\mathrm{F}}\omega}{\sigma^2\Lambda^2\phi^2}}\right), \tag{1}$$

$$K_{\mathrm{P}}(\omega;\boldsymbol{\theta}) = \frac{\gamma P_{\mathrm{F}}/\phi}{\gamma-(\gamma-1)\left(1-\mathrm{i}\frac{\eta\phi}{\rho_{\mathrm{F}}k_0'\omega\mathrm{Pr}}\sqrt{1+\mathrm{i}\frac{4{k_0'}^2\rho_{\mathrm{F}}\omega\mathrm{Pr}}{\eta\Lambda'^2\phi^2}}\right)^{-1}}, \tag{2}$$

where, ω is the radial frequency and $\boldsymbol{\theta} = (\phi, \sigma, \alpha_\infty, \Lambda, \Lambda', k_0')^T$ stand for the parameter vector which describe the acoustic properties of the porous material. The material porosity is given by ϕ, σ measures the flow resistivity, while α_∞ gives its tortuosity. The scalars Λ and Λ' are measures of viscous characteristic length and the thermal characteristic length respectively. Along with the static thermal permeability, ${k_0}'$, the model effectively captures the macroscopic thermal, viscous and inertial characteristics of the porous material. Fluid properties are equally relevant to the acoustical behavior of a porous material and the scalars for fluid mass density ρ_{F}, specific heat ratio γ, dynamic viscosity η, Prandtl number Pr, and equilibrium fluid pressure P_{F} encapsulate the properties of the fluid saturating the porous medium.

The six JCAL parameters are volumetric quantities that describe the acoustic behavior that

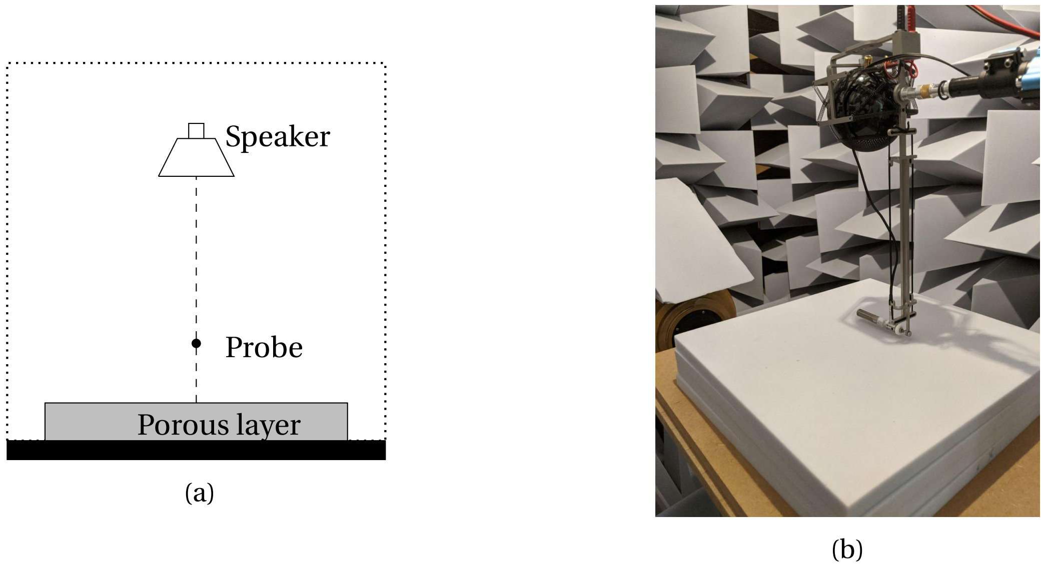

Figure 3: The schematic of the Microflown in situ setup (a) and the apparatus (b) installed in an anechoic chamber.

are not easily measured. While there exist experimental techniques to measure ϕ and σ, there are no standard methodologies for measuring α_∞, Λ, Λ' and k_0'. The surface impedance of a locally-reactive porous layer can be measured more rigorously and be expressed using dynamic density and bulk modulus of the material. Through them, the six JCAL parameters can be defined and this fact is utilized in framing an inverse model to fit to the measured surface impedance.

The experimental setup to measure surface impedance consists of a pressure-particle velocity (PU) probe fixed at a specific distance away from a spherical sound source. The source is attached to a metallic frame with a suspension system composed by multiple springs, isolating structural vibrations from the source to the measuring sensor. The setup is placed at close proximity to the material evaluated along the normal direction as shown in the schematic shown in Figure 3a. While the setup can be used in existing measuring environments, it was placed in an anechoic chamber to eliminate any influence that the surroundings may pose (especially at lower frequencies). The sample is ensured to be flat and made of the same material used in the sensor windscreens. This is necessary to avoid any impact of an oblique angle of incidence on the sample surface and also to minimize the finite-sample effect [15], since the probe coverings are relatively small. The sample was placed against a rigid baffle reflecting all the incident acoustic energy. Figure 3(b) shows the measuring apparatus in an anechoic chamber.

The experimental reflection coefficient $R_{\text{exp}}(\omega)$ of the porous sample was measured using the insitu PU method, assuming that the field is comprised solely of plane waves. The probe measures the acoustic pressure and the particle velocity at its position and the reflection coefficient is computed *a posteriori* using the ratio of the direct acoustic signal from the speaker and the reflected field from the impedance plane. The frequency-dependent surface impedance, $Z_{\text{exp}}(\omega)$ of the porous material is computed based on the measured reflection coefficient $R_{\text{exp}}(\omega)$ using a plane-wave assumption as,

$$Z_{\text{exp}}(\omega) = \frac{1 + R_{\text{exp}}(\omega)}{1 - R_{\text{exp}}(\omega)}. \tag{3}$$

An inverse model is subsequently formulated by evaluating the measured impedance values against the porous parametric model of surface impedance. The parametric surface impedance

$Z(\omega;\boldsymbol{\theta})$ is modeled using a plane wave analysis [29] as,

$$Z(\omega;\boldsymbol{\theta}) = \sqrt{\phi^2 \rho_{\mathrm{P}}(\omega;\boldsymbol{\theta}) K_{\mathrm{P}}(\omega;\boldsymbol{\theta})} \coth\left(\mathrm{i}\frac{\omega^2 \rho_{\mathrm{P}}(\omega;\boldsymbol{\theta})}{K_{\mathrm{P}}(\omega;\boldsymbol{\theta})} l\right), \tag{4}$$

with l as the thickness of the sample. The JCAL parameters are estimated by fitting against the experimental impedance values $Z_{\mathrm{exp},j}(\omega_i)$ measured for $j = 1,\ldots,N$ trials in a sequence of M angular frequencies ω_i, with $i = 1,\ldots,M$, which are equispaced in the logarithmic scale. Hence, the optimal JCAL parameters are given by

$$\boldsymbol{\theta}^\star = \underset{\boldsymbol{\theta}\in(\mathbb{R}^+)^6}{\operatorname{argmin}} \sum_{j=1}^{N} \left(\frac{\sum_{i=1}^{M} |Z_{\mathrm{exp},j}(\omega_i) - Z(\omega_i;\boldsymbol{\theta})|^2}{\sum_{i=1}^{M} |Z_{\mathrm{exp},j}(\omega_i)|^2} \right). \tag{5}$$

The impedance measurements were also conducted at the anechoic chamber at Microflown Technologies. Numerous flat samples of the EKI Melamine and EKI Filter Foam material were obtained from the manufacturer of dimensions $50 \times 60 \times 2\ \mathrm{cm}^3$. Since the samples were relatively thin, each individual layer was observed to exhibit minimal absorption at mid and low frequencies. To quantify the absorptive properties, multiple layers were placed upon each other as is shown in Figure 3(b). The fitting algorithms were implemented in Python using the widely known `scipy` library [30] for optimization and `jax` library [31] for computing derivatives of nonlinear expressions. The absorption coefficient is also computed as a function of the parameters, given as,

$$\alpha(\omega;\boldsymbol{\theta}^\star) = 1 - \left| \frac{Z(\omega,\boldsymbol{\theta}^\star) - \rho_F c_F}{Z(\omega,\boldsymbol{\theta}^\star) + \rho_F c_F} \right|^2, \tag{6}$$

where c_F is the speed of sound.

Figure 4 shows the JCAL parametric fitting performed on the experimental results obtained on the foams. The model considered the multiple layers of the material as a homogenous block of total thickness. The range of the frequencies varied for the materials to ensure a better fit and to avoid non-physical parameter values. The fit shows a qualitative match with the experimental results with a better agreement at frequencies over 1000 Hz. The parameters were obtained by fitting the complex impedance values using a bounded truncated Newton algorithm and Table 1 highlights these estimated parameters. It is noted that the six JCAL parameters over-parameterize the surface impedance measurements, and the porosity, ϕ was fixed during the optimization. Moreover, the inverse optimization with the JCAL model is extremely sensitive to constraints and bounds and can produce atypical non-physical values. The optimization algorithm may be improved with lower parametrization or remodeled cost function or specifically by accomodating other measurement descriptors besides just surface impedance.

Table 1: Fitted JCAL properties to impedance data of the foams

Material	ϕ	α_∞	σ	Λ	Λ'	k_0'
EKI Melamine	0.95	1.1	18443	1.84×10^{-4}	4.07×10^{-4}	1.49×10^{-10}
EKI Filter 90PPI	0.95	1.1	6956	2.58×10^{-4}	1.36×10^{-4}	3.48×10^{-10}

3.1. Finite Element Simulations

To simulate the insertion loss of the two windscreens, finite element techniques were used. Sound transmission over air and via porous layer are modeled as partial differential

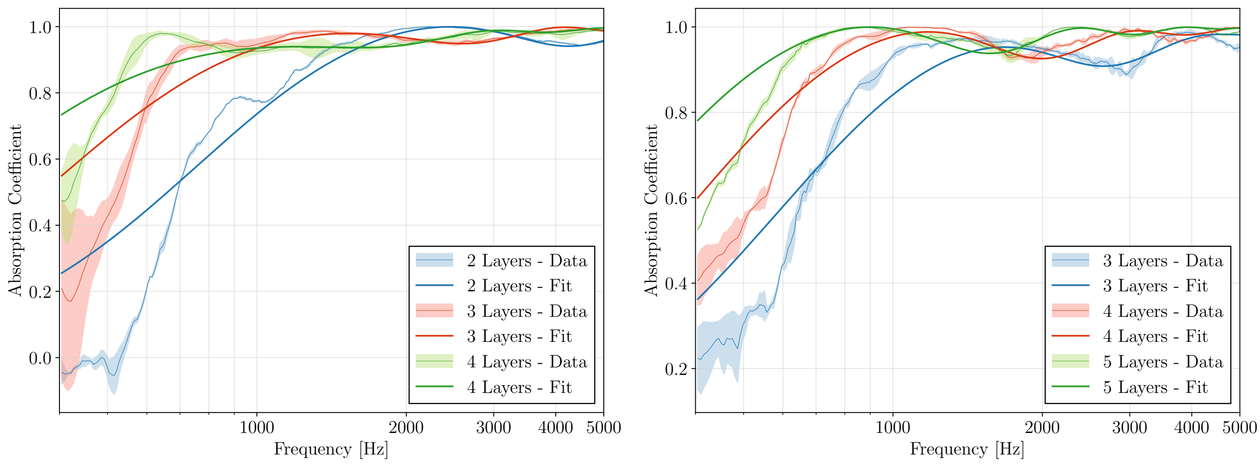

(a) (b)

Figure 4: Absorption measurements for different layers of EKI Melamine (left) and the EKI Filter 90PPI foam (b) with parametric fitting

equations which can be solved using numerical methods. The methodology while elaborate and computationally expensive, can reveal insights into the behaviour of the acoustic fields around the sensor. A sketch of the problem evaluated in this section is displayed in Figure 5, accounting for the probe geometry and the cylindrical porous windscreen. The source is considered as a plane wave emitter with unit pressure amplitude. The impact on the scattered acoustic field due to the probe holder are ignored for the sake of simplification. The anechoic chamber is considered a perfect absorber which does not reflect any waves and the metal probe body is considered rigid. These set of assumptions aid to frame a scattering problem to measure the acoustic field at the position of the sensor through frequency-dependent coupled Helmholtz equations framed using the acoustic displacement field and solved using the finite element method. The Perfectly Matched Layer(PML) technique is used as absorbing boundary conditions. A detailed description regarding the implementation is outside the scope of this work and the reader is referred to [32].

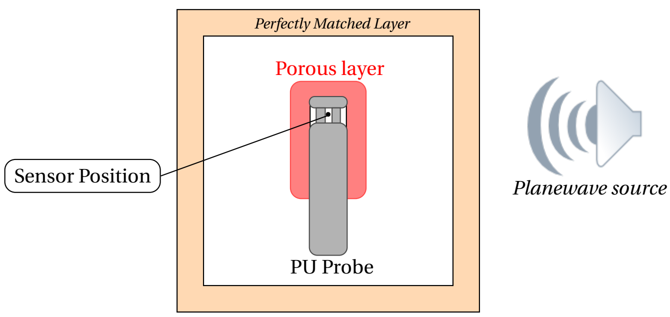

Figure 5: Schematic of the scattering model for measuring insertion loss using the finite element method.

Cylindrical porous layers display a considerable dissipative effect which are numerically characterized using the six JCAL parameters for the material, as described above. The parameters are obtained from the inverse model using the in situ measurement data on flat samples of the same material. The geometric specifications of the probe were measured and introduced into a computer-aided design (CAD) model using SALOME [33]. A 3D Cartesian computational domain of $10.7 \times 10.7 \times 12.5\text{cm}^3$ is made to represent the acoustic fluid around the probe and a scattering problem is formulated to measure the influence of the porous layer around the probe.

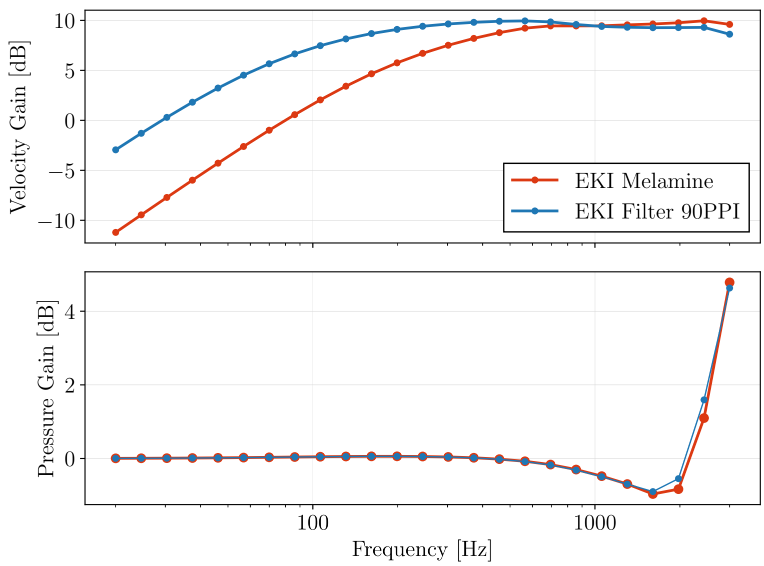

Figure 6: Frequency response comparison of the particle velocity and pressure gain due to both porous layers at the sensor position computed using finite element simulations.

The domain was enveloped by a Cartesian PML of 4.4cm thickness and the domain is discretized into a tetrahedral mesh. The meshes are carefully made conformal with the inner boundaries to ensure the consistency of the dicrete integral formulation.

An incident plane wave of unit magnitude is assumed perpendicular to the direction of the pillars. The complex-valued dynamic porous density and the bulk modulus are computed for each frequency based on the parameters gotten from inverse optimization procedure. Since the plane wave is not a solution to the porous governing equation, care is taken to handle the contribution from the incident plane wave terms on the linear form of the variational equation. Raviart-Thomas finite elements are used to discretize the function spaces and Dirichlet boundary conditions are imposed on the rigid probe boundary. The implementation is performed using FEniCS [34] and the resulting discrete linear system is solved using the MUMPS linear algebra solver. The solution is subsequently post-processed to compute pressure and particle-velocity fields and evaluated at the sensor position. The gains in particle-velocity and pressure at the sensor are denoted by $\boldsymbol{v}_{\text{gain}}$ and p_{gain} respectively and are computed as,

$$\begin{aligned} \boldsymbol{v}_{\text{gain}} &= 10\log_{10}\left(\frac{\boldsymbol{v}_{\text{sensor}}}{\boldsymbol{v}_{\text{ref}}}\right), \\ p_{\text{gain}} &= 10\log_{10}\left(\frac{p_{\text{sensor}}}{p_{\text{ref}}}\right), \end{aligned} \tag{7}$$

where, $\boldsymbol{v}_{\text{sensor}}$ and p_{sensor} are the particle velocity and pressure at the sensor position respectively. The reference particle-velocity $\boldsymbol{v}_{\text{ref}}$ and pressure p_{ref} are taken to the the maximum amplitude of the respective fields due to incident plane wave.

Figure 6 shows the particle velocity and pressure field gains computed at the sensor position for a range of frequencies between 20-1200 Hz in the logarithmic scale. The results emphasize the porous dissipative effects on the flow and a comparison of the plots indicate that the EKI Filter Foam 90PPI windscreen causes a slightly lower impact to the total acoustic field than the EKI Melamine foam for the same thickness.

4. CONCLUSIONS

Designing effecting porous windscreens can aid in superior acoustic measurements especially in outdoor conditions. It should be noted, that the gain effects introduced by the windscreen on sound pressure and particle velocity transducer are fundamentally very different. As such, the design process of windscreen solution for sound intensity probes should carefully consider the effects that it introduces in the acoustic field, both in terms of sound pressure and particle velocity. A thorough study was undertaken to determine the influence of porous material properties on the acoustic sensor through experiments and contrasted with computational tools. The key descriptor studied was the porous insertion loss measured in an anechoic chamber for two different windscreens. The acoustic particle velocity field are seen to be more drastically impacted by foam windscreens relative to the acoustic pressure field. An in-silico workflow was designed to investigate this behavior trying to utilize the material parameters of foam. To this end, a highly parametric model was used to fit against experimentally measured surface impedance of the foam material. The obtained parameters were subsequently used to perform finite element simulations and recreate the impact of insertion loss on the acoustic sensor. Results coroborate the fact that the acoustic particle velocity field is sensitive to porous layer inclusion relative to the pressure field and therefore provide means to quantify the acoustical behavior of porous windscreens.

SOFTWARE

The software materials developed and used in this study are available at https://doi.org/10.5281/zenodo.5171815.

ACKNOWLEDGEMENTS

We gratefully acknowledge the funding received for the "Reduced Order Modelling, Simulation and Optimization of Coupled Systems (ROMSOC)" project from European Union's Horizon 2020 research and innovation programme under Marie Skłodowska-Curie Grant Agreement No. 765374.

REFERENCES

1. J. C. Bleazey. Experimental determination of the effectiveness of microphone wind screens. *Journal of Audio Engineering Society*, 9(1):48–54, 1961.
2. E. B. Brixen and R. Hensen. Wind generated noise in microphones-an overview-part 1. In *Audio Engineering Society Convention 120*. Audio Engineering Society, 2006.
3. W. F. Druyvesteyn and H. E. De Bree. A new sound intensity probe: Comparison to the "pair of pressure microphone" intensity probe. In *Audio Engineering Society Convention 104*. Audio Engineering Society, 1998.
4. H. E. de Bree and E. Tijs. PU nosecone intensity measurements in a wind tunnel. In *German Annual Conference on Acoustics*, 2009.
5. L. E. Thorne. Improvements in topophones or other sound-receiving instruments., U.K. Patent 189725546A, 1897.
6. R. Spotts. Microphone windshield, U.S. Patent 1901065A, 1933.
7. W. D. Phelps. Microphone wind screening. *Radio Corporation of America Reviews*, 111(2):203–12, 1938.
8. R. N. Hosier and P. R. Donavan. Microphone windscreen performance. Technical Report NBS IR 79-1599, National Bureau of Standards, 1979. Edition: 0.
9. J. Wuttke. Microphones and wind. *Journal of the Audio Engineering Society*, 40(10):809–817, 1992.
10. R. Cox, D. Unwin, and T. Sherman. Wind turbine noise impact assessment, where etsu is silent. Technical report, National Wind Watch Inc., 2012.
11. K. Hansen, B. Zajamsek, and C. Hansen. Identification of low frequency wind turbine noise using secondary windscreens of various geometries. *Noise Control Engineering Journal*,

62(2):69–82, 2014.

12. C. Novak, A. Sjostrom, H. Ule, D. Bard, and G. Sandberg. An investigation of different secondary noise wind screen designs for wind turbine noise applications. In *INTER-NOISE and NOISE-CON Congress and Conference Proceedings*, volume 249, pages 5488–5496. Institute of Noise Control Engineering, 2014.
13. C. Kirsch. *Entwicklung und Test eines sekundären Windschirms einschlieš̌lich Kalibrierplatz : Definition einer Abgleichvorschrift für sekundäre Windschirme zum Einsatz bei Schallemissionsmessungen an Windenergieanlagen.* Bachelor thesis, Hochschule Mittweida, University of Applied Sciences, Fakultät Medien, 2017.
14. S. Martens, M. Boas, T. Bohne, and R. Rolfes. Towards the use of secondary windscreens to improve wind turbine sound measurements. In *Proceedings of 15th EAWE PhD Seminar on Wind Energy*, 2019.
15. E. Brandão, A. Lenzi, and S. Paul. A review of the in situ impedance and sound absorption measurement techniques. *Acta Acustica united with Acustica*, 101(3):443–463, 2015.
16. B. G. J. Briere de la Hosseraye. *In situ PU-based characterization of sound absorbing materials for room acoustic modeling purposes.* PhD thesis, 2023.
17. M.A.R Tejeda, P.A. Mendes, R.S. Ribeiro, and P.T. Pinto. In-situ acoustic characterization of porous materials using a pu-probe. In *54º Congreso de Acústica / Tecniacústica 2023*. Sociedad Española de Acústica, 2023.
18. C. Zwikker and C.W. Kosten. *Sound absorbing materials.* Elsevier Pub. Co., 1949.
19. M. A. Delany and E. N. Bazley. Acoustic properties of fibrous absorbent materials. *Applied Acoustics*, 3:105–116, 1970.
20. Y. Miki. Acoustical properties of porous materials, generalization of empirical models. *Journal of the Acoustical Society of Japan (E)*, 11:25–28, 1990.
21. A. Bermúdez, J. L. Ferrín, and A. Prieto. A finite element solution of acoustic propagation in rigid porous media. *International Journal for Numerical Methods in Engineering*, 62(10):1295–1314, 2005.
22. S. Whitaker. Flow in porous media i: A theoretical derivation of darcy's law. *Transport in Porous Media*, 1(1):3–25, 1986.
23. K. Attenborough. Acoustical impedance models for outdoor ground surfaces. *Journal of Sound and Vibration*, 99(4):521–544, 1985.
24. K. Wilson. Relaxation-matched modeling of propagation through porous media, including fractal pore structure. *Journal of the Acoustical Society of America*, 94(2):1136–1145, 1993.
25. D. L. Johnson, J. Koplik, and R. Dashen. Theory of dynamic permeability and tortuosity in fluid-saturated porous media. *Journal of Fluid Mechanics*, 176:379–402, 1987.
26. Y. Champoux and J. F. Allard. Dynamic tortuosity and bulk modulus in air-saturated porous media. *Journal of Applied Physics*, 70(4):1975–1979, 1991.
27. D. Lafarge, P. Lemarinier, J. F. Allard, and V. Tarnow. Dynamic compressibility of air in porous structures at audible frequencies. *Journal of the Acoustical Society of America*, 102:1995–2006, 1997.
28. R. Pride, F. D. Morgan, and A. F. Gangi. Drag forces of porous-medium acoustics. *Bulletin of the American Physical Society*, 47(9):4964–4978, 1993.
29. J. Carbajo, A. Prieto, J. Ramis, and L. Río-Martín. A non-parametric fluid-equivalent approach for the acoustic characterization of rigid porous materials. *Applied Mathematical Modelling*, 76:330–347, 2019.
30. Pauli Virtanen, Ralf Gommers, Travis E. Oliphant, Matt Haberland, Tyler Reddy, David Cournapeau, Evgeni Burovski, Pearu Peterson, Warren Weckesser, Jonathan Bright, Stéfan J.

van der Walt, Matthew Brett, Joshua Wilson, K. Jarrod Millman, Nikolay Mayorov, Andrew R. J. Nelson, Eric Jones, Robert Kern, Eric Larson, C J Carey, İlhan Polat, Yu Feng, Eric W. Moore, Jake VanderPlas, Denis Laxalde, Josef Perktold, Robert Cimrman, Ian Henriksen, E. A. Quintero, Charles R. Harris, Anne M. Archibald, Antônio H. Ribeiro, Fabian Pedregosa, Paul van Mulbregt, and SciPy 1.0 Contributors. SciPy 1.0: Fundamental Algorithms for Scientific Computing in Python. *Nature Methods*, 17:261–272, 2020.

31. James Bradbury, Roy Frostig, Peter Hawkins, Matthew James Johnson, Chris Leary, Dougal Maclaurin, George Necula, Adam Paszke, Jake VanderPlas, Skye Wanderman-Milne, and Qiao Zhang. JAX: composable transformations of Python+NumPy programs, 2018.
32. A. S. Nayak. *Mathematical Modelling and Numerical Simulation of Coupled Acoustic Multi-layer Systems for Enabling Particle Velocity Measurements in the Presence of Airflow*. PhD thesis, 2021.
33. SALOME: An Open-source Integration Platform for Simulation. http://salome-platform.org/.
34. Martin S. Alnæs, Jan Blechta, Johan Hake, August Johansson, Benjamin Kehlet, Anders Logg, Chris Richardson, Johannes Ring, Marie E. Rognes, and Garth N. Wells. The fenics project version 1.5. *Archive of Numerical Software*, 3(100), 2015.